haematologica
Journal of the Ferrata Storti Foundation

Efficacy of DYRK1A inhibitors in novel models of Down syndrome acute lymphoblastic leukemia

by Shannon L. Carey-Smith, Maryam H. Simad, Kunjal Panchal, Carlos Aya-Bonilla, Hannah Smolders, Sang Lin, Jesse D. Armitage, Vivien T. Nguyen, Kathryn Bentley, Jette Ford, Sajla Singh, Joyce Oommen, Anouchka P. Laurent, Thomas Mercher, John D. Crispino, Andrew P. Montgomery, Michael Kassiou, Thierry Besson, Emmanuel Deau, Laurent Meijer, Laurence C. Cheung, Rishi S. Kotecha, and Sébastien Malinge

Received: September 13, 2023.
Accepted: February 19, 2024.

Citation: Shannon L. Carey-Smith, Maryam H. Simad, Kunjal Panchal, Carlos Aya-Bonilla, Hannah Smolders, Sang Lin, Jesse D. Armitage, Vivien T. Nguyen, Kathryn Bentley, Jette Ford, Sajla Singh, Joyce Oommen, Anouchka P. Laurent, Thomas Mercher, John D. Crispino, Andrew P. Montgomery, Michael Kassiou, Thierry Besson, Emmanuel Deau, Laurent Meijer, Laurence C. Cheung, Rishi S. Kotecha, and Sébastien Malinge. Efficacy of DYRK1A inhibitors in novel models of Down syndrome acute lymphoblastic leukemia. Haematologica. 2024 Feb 29. doi: 10.3324/haematol.2023.284271 [Epub ahead of print]

Efficacy of DYRK1A inhibitors in novel models of Down syndrome acute lymphoblastic leukemia

Shannon L. Carey-Smith[1,2,*], Maryam H. Simad[1*], Kunjal Panchal[1,2], Carlos Aya-Bonilla[1], Hannah Smolders[1], Sang Lin[1], Jesse D. Armitage[1], Vivien T. Nguyen[1], Kathryn Bentley[1], Jette Ford[1], Sajla Singh[1], Joyce Oommen[1], Anouchka P. Laurent[3], Thomas Mercher[3], John D. Crispino[4], Andrew P. Montgomery[5], Michael Kassiou[5], Thierry Besson[6], Emmanuel Deau[7], Laurent Meijer[7], Laurence C. Cheung[1,2,8], Rishi S. Kotecha[1,2,9,10] and Sébastien Malinge[1,2,10]

[1]Telethon Kids Cancer Centre, Telethon Kids Institute, Perth, WA, Australia

[2]Curtin Medical School, Curtin University, Perth, WA, Australia

[3]U1170 INSERM, Gustave Roussy, Villejuif, France

[4]Department of Hematology, St Jude Children's Hospital, Memphis, TN, USA

[5]School of Chemistry, University of Sydney, NSW, Australia

[6]University Rouen Normandie, INSA Rouen Normandie, CNRS, COBRA UMR 6014, 76000

[7]Perha Pharmaceuticals, Perharidy Peninsula, Roscoff, France

[8]Curtin Health Innovation Research Institute, Curtin University, Perth, WA, Australia

[9]Department of Clinical Haematology, Oncology, Blood and Marrow Transplantation, Perth Children's Hospital, Perth, WA, Australia

[10]University of Western Australia, Perth, WA, Australia

*SLCS and MHS contributed equally to the study

Corresponding author: Sébastien Malinge, sebastien.malinge@telethonkids.org.au

Short title: Novel DS-ALL models to test DYRK1A inhibitors

Data sharing: RNA sequencing files are available via the Gene Expression Omnibus (GEO) database under the accession number GSE245056.

Acknowledgments

We thank L. Munoz, T. Johns, G. Chua, P. Kumar, T. Lassmann, and staff members of the Bioresources facility at Telethon Kids Institute for their support in obtaining reagents, processing samples and housing/monitoring animals related to this study.

Funding

This research is supported by Australian Government Research Training Program (RTP) Scholarships (SLCS and KP). CAB is supported by a Fellowship from the Jerome Lejeune and Sisley-d'Ornano Foundations. TB supported by the University of Rouen Normandy, INSA Rouen Normandy, the Centre National de la Recherche Scientifique (CNRS), European Regional Development Fund (ERDF), Labex SynOrg (ANR-11-LABX-0029), Carnot Institute I2C, the XL-Chem Graduate School of Research (ANR-18-EURE-0020 XL CHEM), and by Region Normandie. APM is supported by a Postdoctoral Research Fellowship from the University of Sydney's Drug Discovery Initiative. MK is a recipient of a National Health and Medical Research Council Principal Research Fellowship (APP1154692). LM is supported by grants from the Jerome Lejeune Foundation, l'Agence Nationale de la Recherche (ANR) (DYRK-DOWN), BpiFrance (i-Nov, vague 9), the European Union's Horizon 2020 research and innovation programme (Grant #848077) (GO-DS21), and the European Innovation Council (EIC) Accelerator Down-Autonomy project (190138295). SM is supported by a Fellowship from the Cancer Council Western Australia (CCWA). This study was supported by project grants from the Child Cancer Research Foundation (RSK, LCC and SM), Cancer Council Western Australia (Grant #1068) and the Jerome Lejeune Foundation (Grant #1806).

Author contributions

SLCS, MHS and SM conceived and designed the experiments. SLCS, MHS, KP, CAB, HS, SL, JDA, VTN, KB, JF, SS, JO and SM performed the experiments. APL, TM, JDC, TB, APM, MK, ED and LM provided reagents, materials and technical insight. SLCS, MHS, KP, CAB, LCC and RSK significantly contributed to analysis and interpretation of the results. SM supervised the project. SLCS and SM wrote the manuscript. All authors edited and approved the final version of the manuscript for submission.

Disclosures

JDC is a member of the scientific advisory board for Alethiomics, a consultant for Cellarity, and receives research funding from Syndax. LM is a founder of Perha Pharmaceuticals. ED and LM are co-inventors in the Leucettinib patents. RSK discloses advisory board participation from Jazz Pharmaceuticals, Amgen and Link Healthcare.

Despite significant advances, outcomes for children with Down syndrome (DS, trisomy 21) who develop acute lymphoblastic leukemia (ALL) remain poor. Reports of large DS-ALL cohorts have shown that children with DS have inferior event-free survival (EFS) and overall survival (OS) compared to children without DS[1-3]. Children with DS also exhibit increased treatment-related mortality due to infections and toxicities following chemotherapy, higher cumulative risk of relapse and inferior outcomes following relapse[4]. This situation highlights the dire need for the development of more potent and targeted therapies to improve the survival and quality of care for these vulnerable children, who often have additional co-morbidities linked to trisomy 21 that complicates their clinical management. Targeted approaches and immunotherapies have shown promising results for pediatric leukemia[5]. Hence, the development of new models of DS-ALL are needed to rapidly advance drug discovery and refine existing treatment strategies. We recently established DS-ALL patient-derived xenografts (PDXs) and demonstrated that targeting somatic alterations found in DS-ALL using MEK inhibitors combined with conventional treatment has the potential to improve outcome for these children[6]. Targeting the dosage-sensitive mechanisms resulting from the extra copy of chromosome 21 is also an area of intense investigation[7-9]. As such, inhibition of the chromosome 21 kinase DYRK1A using EHT1610 or of its direct targets FOXO1 and STAT3, has shown promising cytotoxic effects both *in vitro* and *in vivo*[8].

In this study, we developed novel clinically relevant models of DS-ALL to facilitate the assessment of new therapeutic agents. First, we modelled oncogenic cooperation seen in DS-ALL *in vitro*[10]. To this end, we transduced wild-type (WT) and trisomic (Tc1) 8-10 week old bone marrow cells with retroviruses encoding the frequently observed mutant $KRAS^{G12D}$ or the more rarely seen BCR-ABL fusion[11] (animal experiments were approved by institutional ethics committee and followed Australian guidelines for the care and use of animals). Of note, the bone marrow stroma and hematopoietic stem cell and progenitor compartment composition did not significantly differ between disomic and trisomic mice, except from an increased proportion of multipotent progenitors MPP2 at the expense of the less committed MPP1 (Fig.S1A-C). Trisomic Tc1 progenitors exhibited increased capacity to form colony-forming unit (CFU)-preB colonies *in vitro* compared to WT (Fig.S1D), as seen previously in the partially trisomic Ts1Rhr (Ts1) model[7]. Ectopic expression of $KRAS^{G12D}$ or BCR-ABL enhanced the number and replating capacity of both WT and Tc1 CFU-preB

colonies compared to the empty vector MIC (MSCV-IRES-mCherry) (Fig.S1E-F). Next, we established two murine DS-ALL cell lines (Tc1-KRAS^{G12D} and Tc1-BCR-ABL), disomic controls (WT-KRAS^{G12D} and WT-BCR-ABL), as well as an independent Ts1/Cdkn2a-KRAS^{G12D} cell line (established from triple transgenic Ts1Rhr, Mb1-Cre, Cdkn2a$^{fl/fl}$ donor mice); although attempts to develop CRLF2-rearranged/JAK2 mutant murine DS-ALL cell lines were unsuccessful. Interestingly, although KRAS^{G12D} led to a constitutive phosphorylation of Erk1/2, the highest levels of Erk1/2 phosphorylation and cytokine independence for cell proliferation were only observed in WT-KRAS^{G12D} cells (Fig.1A-B). All KRAS^{G12D} expressing murine cell lines engrafted in sub-lethally irradiated C57Bl/6 mice in primary and secondary recipients and ultimately succumbed to leukemia with complete penetrance, with recipients displaying mCherry-positive cells in the peripheral blood, bone marrow, and in the spleen (not shown). Engrafted recipient mice exhibited splenomegaly associated with a leukemia-driven disorganized architecture (Fig.S1G-H). We also confirmed that the engrafted cell lines exhibit a phenotype similar to the cell lines cultured *in vitro*; although we noted clonal selection of a CD24^{+}/BP1^{-} pro-B population from the WT-KRAS^{G12D} cells *in vivo*, which was retained in secondary recipients (Fig.1C-D and not shown). Altogether, we developed novel murine models of DS-ALL, providing a unique platform suitable for testing targeted therapies.

To validate the clinical relevance of these murine cells, we focused on the therapeutically targetable chromosome 21 kinase DYRK1A, as recent reports have emphasized its role in childhood leukemia, regardless of Down syndrome[8]. First, we used shRNA interference to show that all five cell lines, disomic (n=2) or trisomic (n=3) and expressing either KRAS^{G12D} or BCR-ABL oncogenes, were sensitive to *Dyrk1a* knock-down (KD) (Fig.2A-B and Fig.S1I). We next assessed the efficacy of new potent DYRK1A inhibitors using a DYRK1A focused library which included EHT1610 used as control, Leucettinib-21 and its inactive isomer (compounds inspired by Leucettines and Leucettamine B, a natural substance produced by the marine sponge *Leucetta microraphis*)[12, 13], and three additional DYRK1A inhibitors whose chemical structure is based on the 7-azaindole scaffold, AM28, AM30 and AM45[14]. In dose-response experiments, we showed that AM30 and Leucettinib-21 were cytotoxic in both Wt-KRAS^{G12D} and Tc1-KRAS^{G12D} cell lines (Fig.2C). We also observed that Leucettinib-21, AM30 and AM45 were more potent than EHT1610 in decreasing cellular growth in all cell lines tested, and

that Tc1-KRAS^{G12D} cells always exhibited lower IC50 values than its disomic counterpart WT-KRAS^{G12D} (Fig.2D-E and Fig.S2A).

To expand our observations, we next established two human DS-ALL cell lines: DS-PER961 and DS-PER962 from our previously reported DS06 (*KRAS*^{G12S}-positive) and DS02 (*CRLF2*-rearranged/*JAK2*^{I682F}-positive) PDXs[6]. These unique models represent the first human cell lines for DS-ALL, with comprehensive characterization at the genomic, transcriptomic and phenotypic levels, confirming their resemblance to the PDX models from which they originated (Fig.3A and Fig.S3A-E). Western blot analyses confirmed phosphorylation of ERK1/2 and STAT5 downstream of KRAS^{G12S} and JAK2^{I682F} mutants in DS-PER961 and DS-PER962 respectively (Fig.3B). Using NOD-SCID-γc-/- (NSG) mice, we also showed that both DS-ALL cell lines engrafted into immunocompromised recipients with DS-PER962 cells being more aggressive than their PDX counterparts (Fig.3C). Using these human cells, we confirmed that Leucettinib-21, AM30 and AM45 were potent inhibitors in human DS-ALL cells and in MHH-CALL4 (a non-DS *CRLF2*-rearranged and JAK2 mutant ALL cell line known to be sensitive to DYRK1A inhibition)(Fig.3D-E and Fig.S2B-D)[8]. No significant effect was seen for AM28 nor for the inactive isomer of Leucettinib-21 (Fig.3D and Fig.S2B-C). Importantly, efficacy of these DYRK1A inhibitors was demonstrated in DS-ALL blasts freshly harvested from four DS-ALL PDX models (described in [6]), validating the suitability of our DS-ALL cells to assess efficacy of new therapies (Fig.3E). Compared to EHT1610 and AM30, Leucettinib-21 was the most potent compound in inhibiting phosphorylation of the known DYRK1A target cyclin D3 in a dose-dependent manner shown in DS-PER962 (Fig.3F), DS-PER961 and in murine cells (Fig.S2E), but had limited effect on FOXO1-phosphorylation (Fig.S2F-I). Next, we evaluated *in vitro* drug combinations of Leucettinib-21 with targeted and conventional therapies and identified synergy with vincristine and an additive effect with dexamethasone and L-asparaginase (Fig.3G and Fig.S2J). An additive effect between Leucettinib-21 and the targeted therapies ruxolitinib (a JAK1/2 inhibitor) and trametinib (a MEK1/2 inhibitor) was also seen in DS-PER962 (CRLF2-positive/JAK2^{I682F} mutant) and in the DS-PER961 (KRAS^{G12S}) cell lines, respectively (Fig.3G). Finally, we assessed the efficacy of Leucettinib-21 *in vivo* in the DS06 and DS02 PDX models and observed that *in vivo* treatment with Leucettinib-21 decreased leukemia burden but did not fully eradicate leukemia (Fig.3H). Together, this data demonstrates the suitability and clinical relevance of the novel murine and human models we have established and emphasizes the key role of DYRK1A in DS-ALL.

Compared to other children, higher sensitivity to treatment-related toxicity in children with DS-ALL remains a major clinical challenge. This has significantly limited the development of novel targeted therapies for this patient population, ultimately delaying translation into clinical trials. Recently, integration of immunotherapeutic approaches has offered promise in reducing toxicity. Laetsch *et al*. reported promising comparable outcomes between DS- and non-DS children with relapsed/refractory B-ALL who received CD19-directed chimeric antigen receptor T-cell therapy, including similar rates of CD19-negative relapse[15], and an ongoing clinical trial is currently assessing whether blinatumomab can replace two blocks of consolidation chemotherapy for treatment of *de novo* DS-ALL (NCT03911128). As an alternative approach, identifying key vulnerabilities in DS-ALL blasts could provide the molecular basis for development of novel targeted therapies. While resources such as the recent in-depth characterization of the genetic landscape of DS-ALL can provide such insight[10], we have developed novel models of DS-ALL and shown that inhibiting the dosage-sensitive mechanisms altered by trisomy 21 may also represent a new avenue to integrate agents with low toxicity and ultimately improve outcomes and quality of care for children with DS-ALL. We demonstrated that a reduction in *DYRK1A* expression is sufficient to decrease the growth of DS-ALL cell lines, confirmed the sensitivity of human and murine cells to DYRK1A inhibition and showed that the leading candidate, Leucettinib-21, potentiates the cytotoxic effect of other chemotherapeutic and targeted agents and delayed leukemia expansion *in vivo*, with no detectable toxicity identified in the peripheral blood (Fig.S2K). Leucettinib-21 has recently completed regulatory preclinical safety studies and is primed for early phase clinical assessment. Strikingly, studies have demonstrated the preclinical impact of targeting DYRK1A activity in different subtypes of childhood leukemia[8], further emphasizing the potential benefit for investigating Leucettinib-21 or other new potent DYRK1A inhibitors in clinical trials for ALL.

Altogether, this study has established and comprehensively characterized the first DS-ALL cell lines, providing suitable and clinically relevant cellular models to identify new molecular weaknesses in DS-ALL and test the efficacy of novel targeted therapies (as exemplified here with DYRK1A inhibition), alone or in combination with standard of care, to ultimately develop new, less toxic treatments to improve the outcome for children with DS-ALL.

References

1. Buitenkamp TD, Izraeli S, Zimmermann M, et al. Acute lymphoblastic leukemia in children with Down syndrome: a retrospective analysis from the Ponte di Legno study group. Blood. 2014;123(1):70-77.
2. Ceppi F, Stephens D, den Hollander BS, et al. Clinical presentation and risk factors of serious infections in children with Down syndrome treated for acute lymphoblastic leukemia. Pediatr Blood Cancer. 2016;63(11):1949-1953.
3. Rabin KR, Devidas M, Chen Z, et al. Outcomes in Children, Adolescents, and Young Adults With Down Syndrome and ALL: A Report From the Children's Oncology Group. J Clin Oncol. 2024;42(2):218-227.
4. Meyr F, Escherich G, Mann G, et al. Outcomes of treatment for relapsed acute lymphoblastic leukaemia in children with Down syndrome. Br J Haematol. 2013;162(1):98-106.
5. Rafei H, Kantarjian HM, Jabbour EJ. Targeted therapy paves the way for the cure of acute lymphoblastic leukaemia. Br J Haematol. 2020;188(2):207-223.
6. Laurent AP, Siret A, Ignacimouttou C, et al. Constitutive Activation of RAS/MAPK Pathway Cooperates with Trisomy 21 and Is Therapeutically Exploitable in Down Syndrome B-cell Leukemia. Clin Cancer Res. 2020;26(13):3307-3318.
7. Lane AA, Chapuy B, Lin CY, et al. Triplication of a 21q22 region contributes to B cell transformation through HMGN1 overexpression and loss of histone H3 Lys27 trimethylation. Nat Genet. 2014;46(6):618-623.
8. Bhansali RS, Rammohan M, Lee P, et al. DYRK1A regulates B cell acute lymphoblastic leukemia through phosphorylation of FOXO1 and STAT3. J Clin Invest. 2021;131(1):e135937.
9. Page EC, Heatley SL, Eadie LN, et al. HMGN1 plays a significant role in CRLF2 driven Down Syndrome leukemia and provides a potential therapeutic target in this high-risk cohort. Oncogene. 2022;41(6):797-808.
10. Li Z, Chang TC, Junco JJ, et al. Genomic landscape of Down syndrome-associated acute lymphoblastic leukemia. Blood. 2023;142(2):172-184.
11. O'Doherty A, Ruf S, Mulligan C, et al. An aneuploid mouse strain carrying human chromosome 21 with Down syndrome phenotypes. Science. 2005;309(5743):2033-2037.
12. Tahtouh T, Durieu E, Villiers B, et al. Structure-Activity Relationship in the Leucettine Family of Kinase Inhibitors. J Med Chem. 2022;65(2):1396-1417.
13. Lindberg MF, Deau E, Miege F, et al. Chemical, Biochemical, Cellular, and Physiological Characterization of Leucettinib-21, a Down Syndrome and Alzheimer's Disease Drug Candidate. J Med Chem. 2023;66(23):15648-15670.
14. Zhou Q, Phoa AF, Abbassi RH, et al. Structural Optimization and Pharmacological Evaluation of Inhibitors Targeting Dual-Specificity Tyrosine Phosphorylation-Regulated Kinases (DYRK) and CDC-like kinases (CLK) in Glioblastoma. J Med Chem. 2017;60(5):2052-2070.
15. Laetsch TW, Maude SL, Balduzzi A, et al. Tisagenlecleucel in pediatric and young adult patients with Down syndrome-associated relapsed/refractory acute lymphoblastic leukemia. Leukemia. 2022;36(6):1508-1515.

Figure Legends

Figure 1: Establishment of novel DS-ALL models for preclinical testing.

A. Constitutive phosphorylation of Stat5 and Erk1/2 in $KRAS^{G12D}$ and BCR-ABL expressing murine cells (starved for 6 hours). **B.** Growth of murine WT-$KRAS^{G12D}$, Tc1-$KRAS^{G12D}$ and Ts1/Cdkn2a-$KRAS^{G12D}$ cells with or without cytokines (Il-7, Scf and Flt3-L, 10ng/ml) over 6 days. **C.** Kaplan-Meier analysis comparing survival of primary (1R) and secondary (2R) sub-lethally irradiated recipient mice engrafted with 1-2x10^6 Tc1-$KRAS^{G12D}$ (1R n=4, 2R n=6), Wt-$KRAS^{G12D}$ (1R n=5, 2R n=6) and Ts1Rhr/Cdkn2a-$KRAS^{G12D}$ (1R n=5, 2R n=6) cell lines; $^{**}p<0.01$. **D.** Phenotype of the murine cell lines assessing surface expression of BP1 and CD24 (phenotype of the WT-BCR-ABL and Tc1-BCR-ABL cell lines are in supplemental Fig.1F). **F.** Representative flow plots showing phenotype of mCherry-positive cell lines in primary and secondary recipients.

Figure 2: Genetic and pharmacological inhibition of DYRK1A decreases growth of DS-ALL cells.

A. Ratio of WT-$KRAS^{G12D}$ and Tc1-$KRAS^{G12D}$ transduced with GFP-expressing Banshee vectors encoding two shDyrk1a compared to empty Banshee-U6 counterparts over 9 days (n=4 replicates); $^{***}p<0.001$. **B.** Validation of Dyrk1a knock-down at the protein level 48 hours after transduction (GFP-sorted). DYRK1A band intensities were quantified and normalized as a ratio of shDyrk1a-transduced to control U6-transduced WT-$KRAS^{G12D}$ cells. **C.** Cytotoxic effect of increasing doses of the DYRK1A inhibitors EHT1610, AM30, Leucettinib-21 (LCTB-21) and its inactive isomer iso-Leucettinib-21 (Iso LCTB-21) at 48 hours in murine WT-$KRAS^{G12D}$ and Tc1-$KRAS^{G12D}$ cells assessed by flow cytometry (AnnexinV-staining). **D.** Dose-response curves assessing efficacy of EHT1610, LCTB-21 and Iso LCTB-21 at 72 hours by alamarBlue cell viability assay in murine WT-$KRAS^{G12D}$ and Tc1-$KRAS^{G12D}$ cells. **E.** Heatmap integrating relative IC50 values obtained for the DYRK1A inhibitors tested in our murine cell lines.

Figure 3: Efficacy of DYRK1A inhibition in novel human DS-ALL cell lines and patient-derived xenograft models.

A. Representative flow plots assessing CD38 and TSLPR expression of the human DS-PER962 and DS-PER961 DS-ALL cell lines compared to their corresponding DS06 and DS02 patient-derived xenografts (PDXs), and to NSG recipients engrafted with $1x10^6$ DS-ALL cell lines (PDX^{cells}). **B.** Western blots assessing the constitutive phosphorylation of JAK2, STAT5 and ERK1/2 in DS-PER962 and DS-PER961 cell lines following a 6 hour starvation; the non-DS MHH-CALL4 (CRLF2-rearranged/*JAK2* mutant) ALL cell line was used as control. **C.** Kaplan-Meier curves comparing the survival of the DS-PER962 and DS-PER961 PDXs (n=3-4) to their corresponding DS02 and DS06 PDXs (n=9-12); ***p<0.001. **D.** Efficacy of EHT1610, Leucettinib-21 (LCTB-21) and its inactive isomer iso-Leucettinib-21 (Iso LCTB-21) in the human DS-PER962 and DS-PER961 cell lines (72 hours). **E.** Heatmap representing the relative IC50 values obtained in the non-DS-ALL, DS-ALL human cell lines and DS-ALL cells freshly harvested from PDX models (n=6-8). **F.** Western blot comparing the effect of EHT1610, LCTB-21 and AM30 on phospho-cyclin D3 and total cyclin D3 stability after 6 hours of treatment in the DS-PER962 cell line. **G.** ZIP scores obtained from combining Leucettinib-21 (10 doses from 0.01 to 10µM) with trametinib (0.0001-20µM), ruxolitinib (0.0001-20µM), vincristine (0.0005-0.5µM), dexamethasone (0.00025-20µM) and L-asparaginase (0.1-20µM) in the human DS-ALL cell lines. ZIP scores < -10 = antagonism; -10 to 10 = additive; > 10 = synergy. **H.** *In vivo* effect of Leucettinib-21 on leukemia burden in the peripheral blood of the DS02 and DS06 PDX models (oral gavage, 2 weeks and 4 weeks of treatment respectively); *p<0.05, **p<0.01.

Figure 1

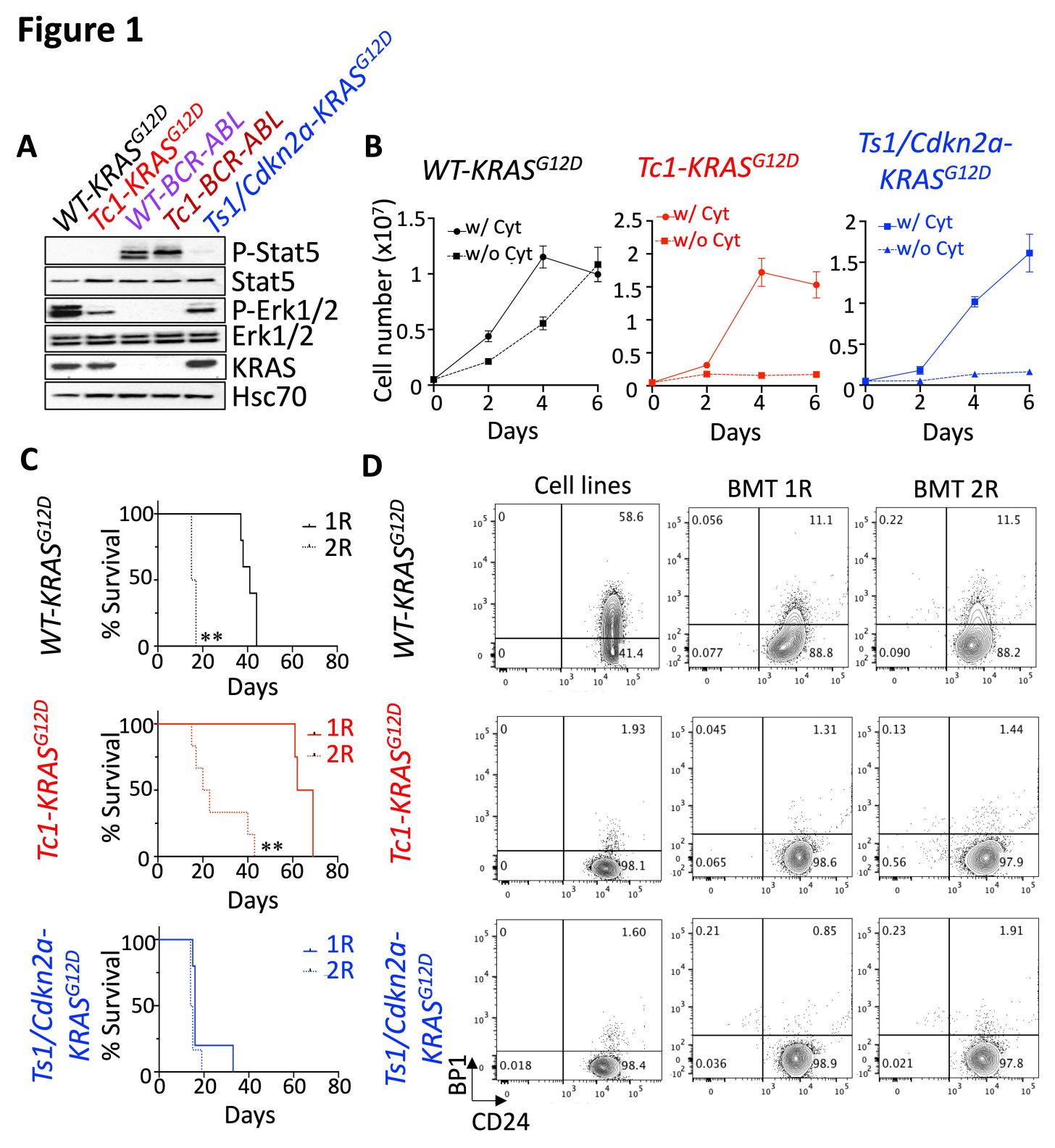
A
WT-KRASG12D
Tc1-KRASG12D
WT-BCR-ABL
Tc1-BCR-ABL
Ts1/Cdkn2a-KRASG12D
P-Stat5
Stat5
P-Erk1/2
Erk1/2
KRAS
Hsc70
B
WT-KRASG12D
Tc1-KRASG12D
Ts1/Cdkn2a-KRASG12D
Cell number (x10^7)
w/ Cyt
w/o Cyt
Days
C
WT-KRASG12D
Tc1-KRASG12D
Ts1/Cdkn2a-KRASG12D
% Survival
1R
2R
**
Days
D
Cell lines
BMT 1R
BMT 2R
WT-KRASG12D
Tc1-KRASG12D
Ts1/Cdkn2a-KRASG12D
58.6
41.4
11.1
88.8
11.5
88.2
1.93
98.1
1.31
98.6
1.44
97.9
1.60
98.4
0.85
98.9
1.91
97.8
BP1
CD24

Figure 2

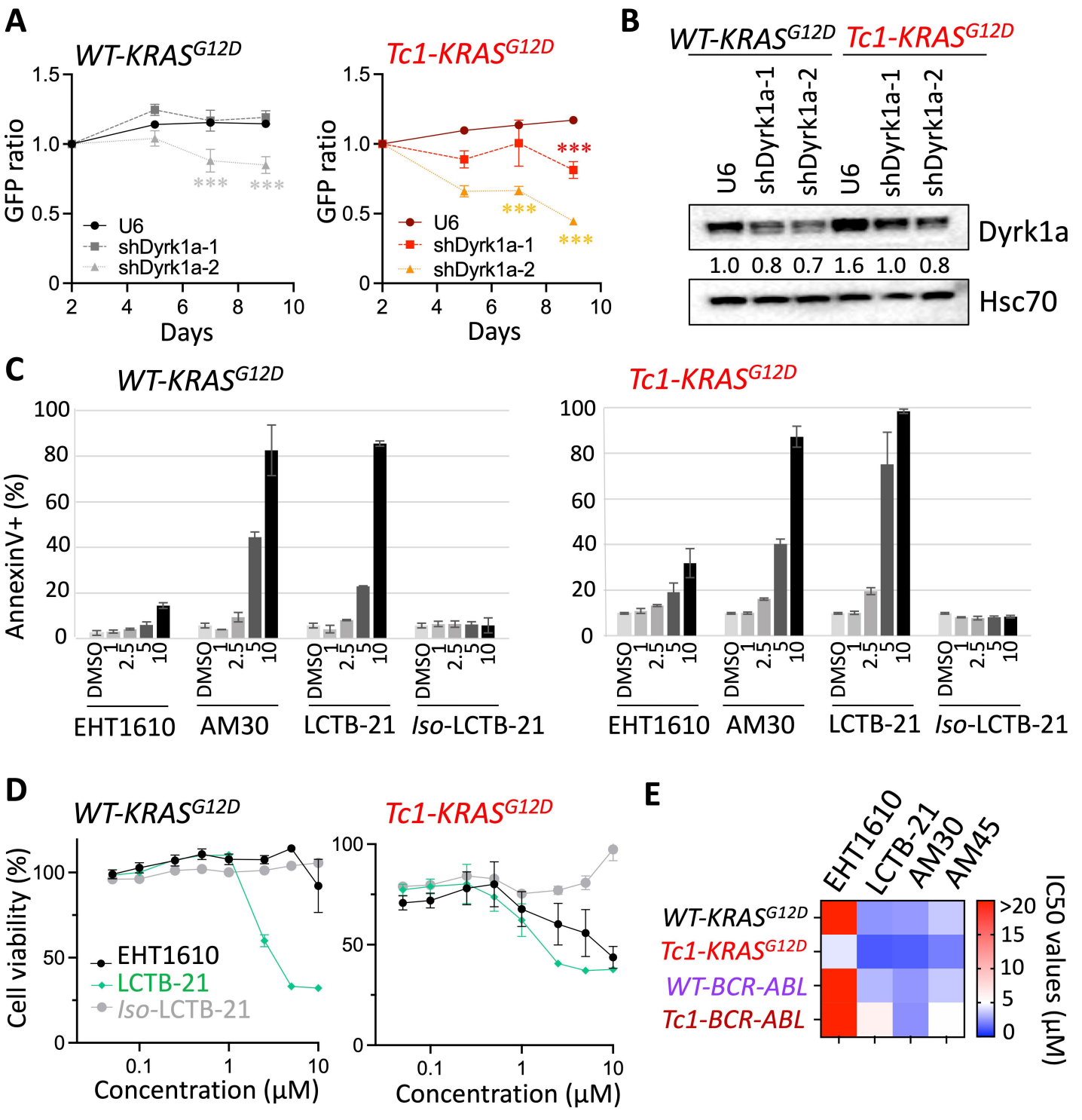
A
WT-KRASG12D
Tc1-KRASG12D
GFP ratio
Days
U6
shDyrk1a-1
shDyrk1a-2
***
B
WT-KRASG12D
Tc1-KRASG12D
U6
shDyrk1a-1
shDyrk1a-2
Dyrk1a
1.0 0.8 0.7 1.6 1.0 0.8
Hsc70
C
WT-KRASG12D
Tc1-KRASG12D
AnnexinV+ (%)
DMSO
1
2.5
5
10
EHT1610
AM30
LCTB-21
Iso-LCTB-21
D
WT-KRASG12D
Tc1-KRASG12D
Cell viability (%)
EHT1610
LCTB-21
Iso-LCTB-21
Concentration (μM)
E
EHT1610
LCTB-21
AM30
AM45
WT-KRASG12D
Tc1-KRASG12D
WT-BCR-ABL
Tc1-BCR-ABL
IC50 values (μM)
>20
15
10
5
0

Figure 3

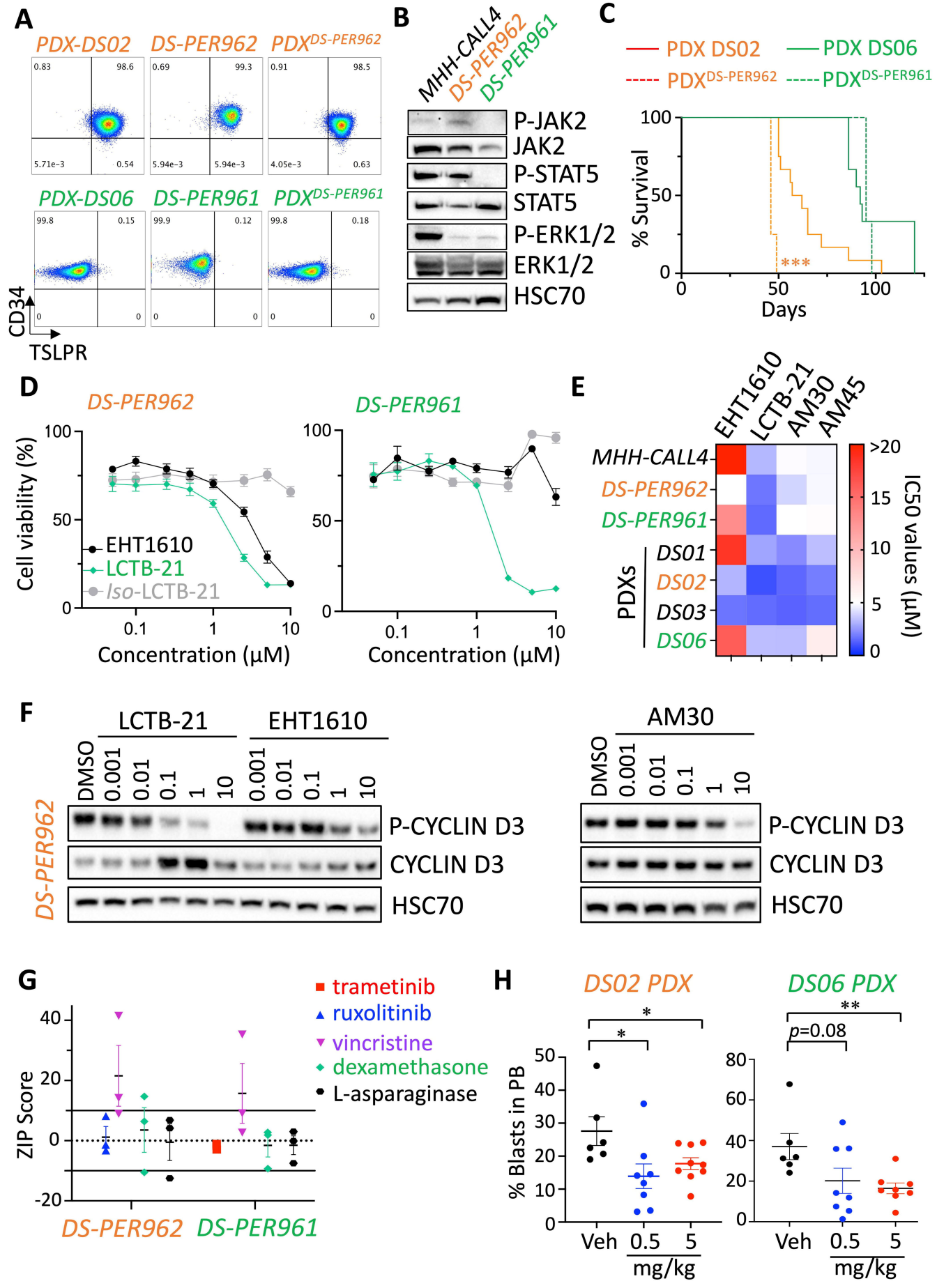
A
PDX-DS02
DS-PER962
PDXDS-PER962
PDX-DS06
DS-PER961
PDXDS-PER961
CD34
TSLPR
B
MHH-CALL4
DS-PER962
DS-PER961
P-JAK2
JAK2
P-STAT5
STAT5
P-ERK1/2
ERK1/2
HSC70
C
PDX DS02
PDX DS06
PDXDS-PER962
PDXDS-PER961
% Survival
Days
***
D
DS-PER962
DS-PER961
Cell viability (%)
EHT1610
LCTB-21
Iso-LCTB-21
Concentration (μM)
E
EHT1610
LCTB-21
AM30
AM45
MHH-CALL4
DS-PER962
DS-PER961
PDXs
DS01
DS02
DS03
DS06
IC50 values (μM)
F
LCTB-21
EHT1610
AM30
DMSO
DS-PER962
P-CYCLIN D3
CYCLIN D3
HSC70
G
trametinib
ruxolitinib
vincristine
dexamethasone
L-asparaginase
ZIP Score
DS-PER962
DS-PER961
H
DS02 PDX
DS06 PDX
% Blasts in PB
p=0.08
Veh
0.5
5
mg/kg

Efficacy of DYRK1A inhibitors in novel models of Down syndrome acute lymphoblastic leukemia

Shannon L. Carey-Smith[1,2,*], Maryam H. Simad[1*], Kunjal Panchal[1,2], Carlos Aya-Bonilla[1], Hannah Smolders[1], Sang Lin[1], Jesse D. Armitage[1], Vivien T. Nguyen[1], Kathryn Bentley[1], Jette Ford[1], Sajla Singh[1], Joyce Oommen[1], Anouchka P. Laurent[3], Thomas Mercher[3], John D. Crispino[4], Andrew P. Montgomery[5], Michael Kassiou[5], Thierry Besson[6], Emmanuel Deau[7], Laurent Meijer[7], Laurence C. Cheung[1,2,8], Rishi S. Kotecha[1,2,9,10] and Sébastien Malinge[1,2,10]

[1]Telethon Kids Cancer Centre, Telethon Kids Institute, Perth, WA, Australia

[2]Curtin Medical School, Curtin University, Perth, WA, Australia

[3]U1170 INSERM, Gustave Roussy, Villejuif, France

[4]Department of Hematology, St Jude Children`s Hospital, Memphis, TN, USA

[5]School of Chemistry, University of Sydney, NSW, Australia

[6]University Rouen Normandie, INSA Rouen Normandie, CNRS, COBRA UMR 6014, 76000 Rouen, France

[7]Perha Pharmaceuticals, Perharidy Peninsula, Roscoff, France

[8]Curtin Health Innovation Research Institute, Curtin University, Perth, WA, Australia

[9]Department of Clinical Haematology, Oncology, Blood and Marrow Transplantation, Perth Children's Hospital, Perth, WA, Australia

[10]University of Western Australia, Perth, WA, Australia

*SLCS and MHS contributed equally to the study

Supplementary Figures and legends

Supplementary Figure 1

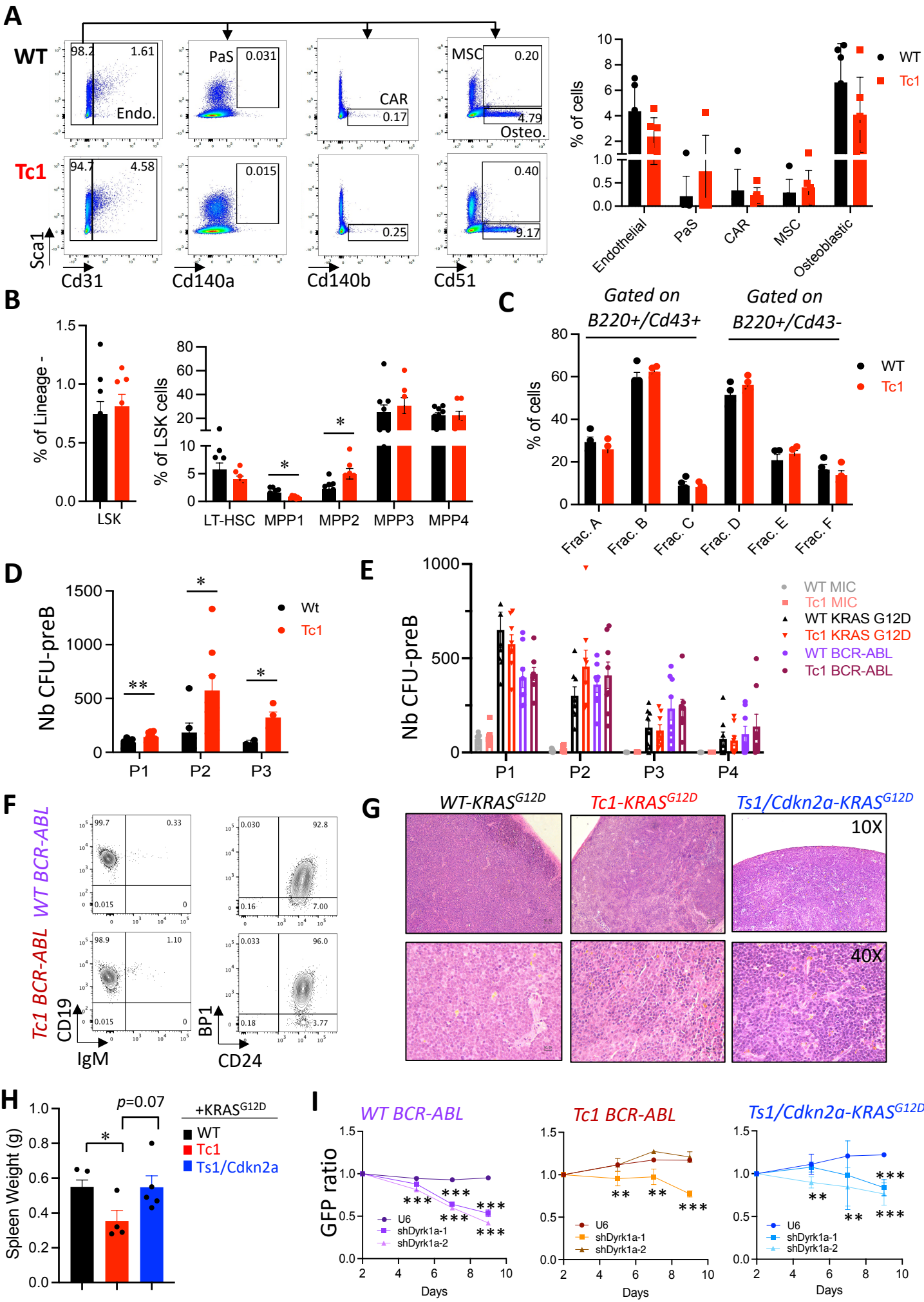

Supplementary Figure 1: Establishment of murine DS-ALL cells.

A. Representative flow plots comparing the bone marrow stroma of 8-10 week old wild-type (WT) and trisomic (Tc1) mice, gated on CD45-Ter119- and depicting the percentage of endothelial cells (endo, CD31-positive), CD31-negative PaS (PDGFRa(Cd140a)+/Sca1+), Cxcl12-abundant reticular cells (CAR, PDGFRb(cd140b)+/Sca1-), mesenchymal stem cells (MSC, Sca1+/CD51+) and osteoblastic cells (osteo, Sca1-/CD51+). *Right panel*: box plot integrating all data (n=6). **B.** Bar graph displaying the percentage of the different hematopoietic stem cells and progenitors in 8-10 week old mice (n=7-9); *p<0.05. LSK = Lineage-negative/Sca1+/Kit+, LT-HSC (Long-term hematopoietic stem cells, LSK+CD34-FLT3-CD150+CD48-), MPP1 (multipotent progenitor 1, LSK+CD34+FLT3-CD150+CD48-), MPP2 (LSK+CD34+FLT3-CD150+CD48+), MPP3 (LSK+CD34+FLT3-CD150-CD48+), MPP4 (LSK+CD34+FLT3+CD150-CD48+). **C.** Bar graph displaying the proportion of the hardy fraction in the bone marrow of WT and Tc1 mice (n=4); Fraction A (B220+CD43+CD24-BP1-), Fraction B (B220+CD43+CD24+BP1-), Fraction C (B220+CD43+CD24+BP1+), Fraction D (B220+CD43-IgM-IgD-), Fraction E (B220+CD43-IgM+IgD-) and Fraction F (B220+CD43-IgM+IgD+). **D.** Number of colony-forming unit (CFU)-preB colonies obtained from 8-10 week old WT and Tc1 donor bone marrow cells over 3 passages (n=8-9); *p<0.05, **p<0.01. **E.** Number of CFU-preB colonies obtained from sorted mCherry-positive bone marrow progenitor cells transduced with $KRAS^{G12D}$, BCR-ABL retroviruses compared to empty vector retroviruses (MIC = MSCV-IRES-mCherry), over 4 passages (n=8). **F.** Phenotype of the WT-BCR-ABL and Tc1-BCR-ABL cell lines assessing surface expression of CD19, IgM, BP1 and CD24. **G.** Representative spleen sections from WT-$KRAS^{G12D}$, Tc1-$KRAS^{G12D}$ and Ts1/cdkn2a-$KRAS^{G12D}$ primary recipients, stained with hematoxylin and eosin (10X and 40X magnification). **H.** Average spleen weight at endpoint in WT-$KRAS^{G12D}$ (n=5), Tc1-$KRAS^{G12D}$ (n=4) and Ts1/Cdkn2a-$KRAS^{G12D}$ (n=5) irradiated recipient mice; *p<0.05. **I.** Ratio of GFP-expressing Banshee vectors encoding two shDyrk1a compared to empty Banshee-U6 counterparts over 9 days in the murine WT-BCR-ABL, Tc1-BCR-ABL and Ts1/cdkn2a-$KRAS^{G12D}$ cells (n=4 replicates); **p<0.01, ***p<0.001.

Supplementary Figure 2

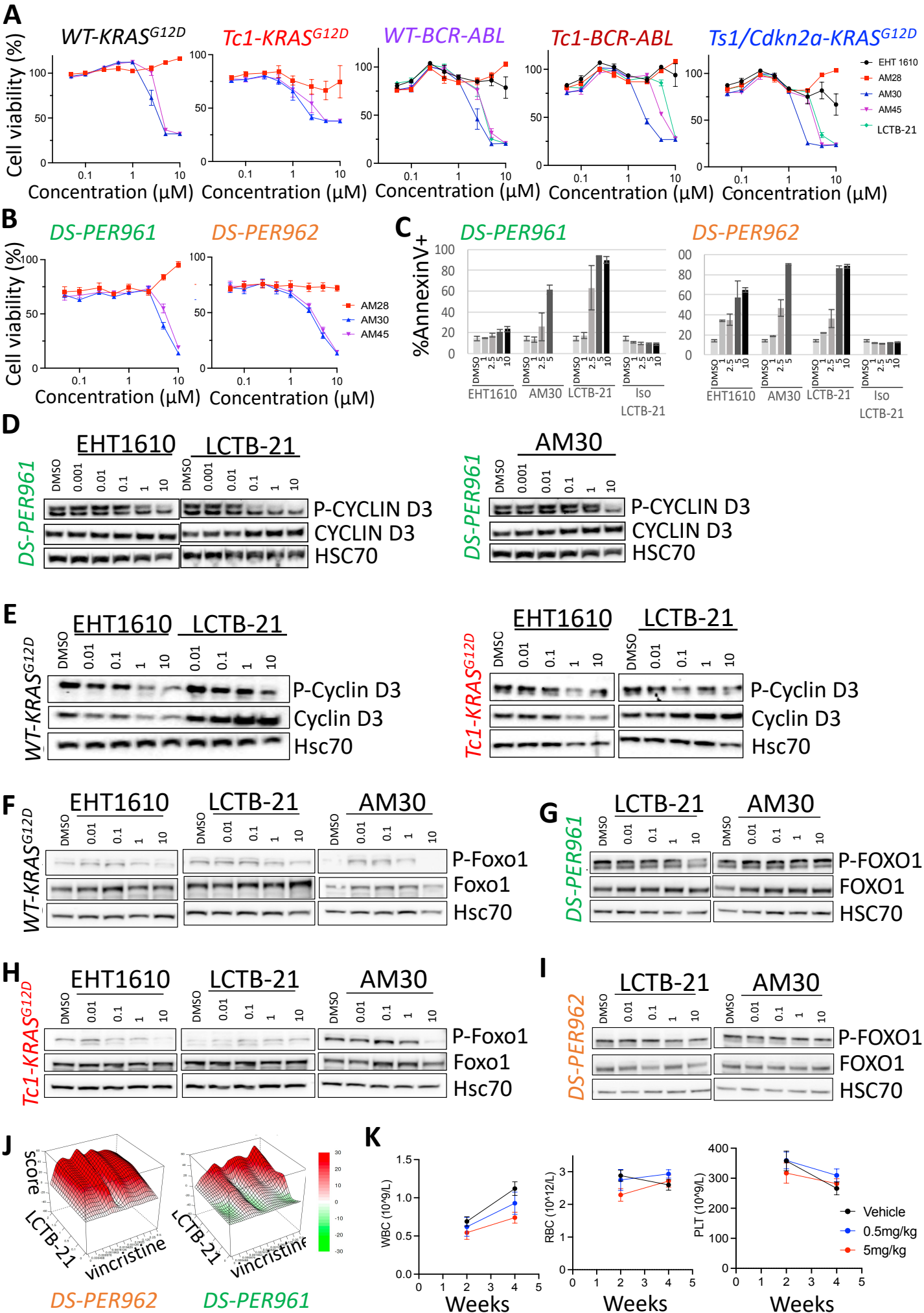

Supplementary Figure 2: Preclinical testing of new DYRK1A inhibitors in non-DS and DS-ALL.

A. Dose-response curves for EHT1610, Leucettinib-21 (LCTB-21), AM28, AM30 and AM45 in murine cell lines. **B.** Dose-response curves for AM28, AM30 and AM45 in human DS-PER961 and DS-PER962 cell lines. **C.** Bar graphs showing the impact of increasing doses 1µM, 2.5µM, 5µM and 10µM of the DYRK1A inhibitors EHT1610, AM30, LCTB-21 and its inactive isomer iso-Leucettinib-21 (Iso LCTB-21) on cell viability of DS-PER961 and DS-PER962 at 48 hours assessed by flow cytometry (AnnexinV-positive cells). **D.** Western blots of phospho-Cyclin D3 performed from protein extracted from the DS-PER961 human cell line after a 6 hour treatment with increasing doses (in µM) of the DYRK1A inhibitors EHT1610, Leucettinib-21 and AM30, compared to treatment with DMSO. **E.** Western blots of phospho-Cyclin D3 performed from protein extracted from WT-KRAS^{G12D} and Tc1-KRAS^{G12D} murine cells after a 6 hour treatment with increasing doses (in µM) of the DYRK1A inhibitors EHT1610 and Leucettinib-21, compared to treatment with DMSO. **F-I.** Assessment of FOXO1 (Ser326) phosphorylation in response to DYRK1A inhibition (6 hour treatment) in (**F**) murine WT-KRAS^{G12D}, (**G**) human DS-PER961 (KRAS^{G12S}), (**H**) murine Tc1-KRAS^{G12D} and (**I**) human DS-PER962 (CRLF2-rearranged/JAK2^{I682F}) cells. **J.** Representative plots showing synergy between LCTB-21 and vincristine in DS-PER962 and DS-PER961 cell lines. **K.** Blood count assessment showing WBC (white blood cell count), RBC (red blood cell count) and PLT (platelet counts) at week 2 and week 4 of treatment with 0.5 mg/kg and 5 mg/kg of Leucettinib-21 compared to vehicle in the DS06 patient-derived xenograft (n=3 per group and per timepoint).

Supplementary Figure 3

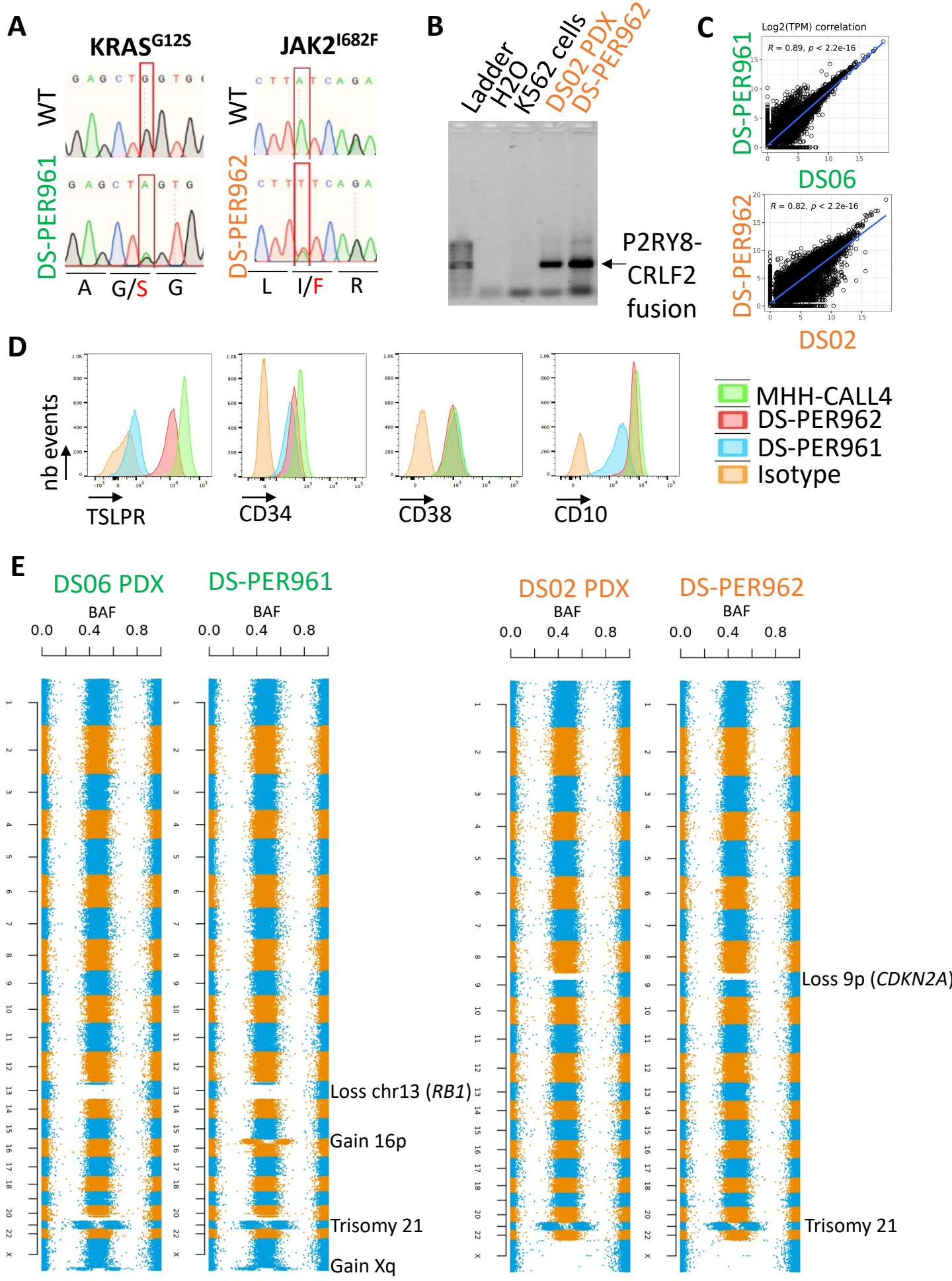

Supplementary Figure 3: Characterization of human DS-ALL cell lines.

A. Sanger sequencing of genomic DNA confirming the presence of the *KRAS*^{G12S} and *JAK2*^{I682F} mutations found in the DS-PER961 and DS-PER962 cell lines respectively. **B.** Validation of the P2RY8-CRLF2 fusion transcript in the DS02 patient-derived xenograft (PDX) and DS-PER962 cell line compared to K562 control cells (primer sequences are indicated in supplemental table 2). **C.** Spearman correlation of the transcriptional profiles obtained in the DS-PER961 and DS-PER962 cell lines (Y-axis) compared to the PDX model they originate from (X-axis). RNA sequencing files are available via the Gene Expression Omnibus (GEO) database under the accession number GSE245056. **D.** Representative flow plots comparing the Mean Fluorescence Intensity (MFI) for the surface markers TSLPR, CD34, CD38 and CD10 in the DS-PER961 (in blue) and DS-PER962 (in red) compared to MHH-CALL4 cells (in green); isotypes are represented in orange. **E.** Bi-allelic frequencies obtained from SNP arrays (HumanCytoSNP-12 BeadChip (HumanCytoSNP-12v2.1; Illumina) comparing DS-PER961 and DS-PER962 cell lines with the PDX they originate from, showing that the cell lines are relatively stable at the genomic level.